Temperature-dependent and optimized thermal emission by spheres

K.L. Nguyen, O. Merchiers, and P.-O. Chapuis

Citation: Appl. Phys. Lett. **112**, 111906 (2018); doi: 10.1063/1.5010426
View online: https://doi.org/10.1063/1.5010426
View Table of Contents: http://aip.scitation.org/toc/apl/112/11
Published by the American Institute of Physics

APPLIED PHYSICS LETTERS 112, 111906 (2018)

Temperature-dependent and optimized thermal emission by spheres

K.L. Nguyen,[a)] O. Merchiers, and P.-O. Chapuis
University Lyon, CNRS, INSA-Lyon, Université Claude Bernard Lyon 1, CETHIL UMR5008, F-69621 Villeurbanne, France

(Received 25 October 2017; accepted 28 February 2018; published online 14 March 2018)

We investigate the temperature and size dependencies of thermal emission by homogeneous spheres as a function of their dielectric properties. Different power laws obtained in this work show that the emitted power can depart strongly from the usual fourth power of temperature given by Planck's law and from the square or the cube of the radius. We also show how to optimize the thermal emission by selecting permittivities leading to resonances, which allow for the so-called super-Planckian regime. These results will be useful as spheres, i.e. the simplest finite objects, are often considered as building blocks of more complex objects. *Published by AIP Publishing.*
https://doi.org/10.1063/1.5010426

Thermal emission by spheres is key to understanding the radiative properties of more complex micro- and nanostructures. In scanning thermal microscopy and thermal-radiation scanning tunnelling microscopy, the tip of the probe can sometimes be approximated by a sphere.[1–3] In Refs. 4 and 5, spheres attached to tips were used for experimental investigations of near-field thermal radiation. Finally, incandescent soot particles and also aerosols are often assumed to be made of spherical emitters.[6] Hence, spherical emitters are useful tools to describe a wide variety of phenomena but are also interesting in their own right. It has been predicted that spheres can radiate more energy than what is expected for a blackbody.[7–9] This phenomenon was also observed for cylinders[10] and meta-materials.[11,12] Until now, however, there has been no thorough analysis on how the temperature and size dependencies influence the emission properties of spheres. Furthermore, no useful criteria have been proposed to achieve super-Planckian emission (see Fig. 1) in usual materials. To fill in this gap, we discuss size and temperature dependencies of the radiative emission of dielectric and metallic spheres. We show that the temperature dependence departs strongly from the well-known fourth power associated with the Stefan-Boltzmann law. We discriminate between the effects linked to the particle size, explained by means of the Mie theory, and those linked to the dielectric functions. In particular, we analyze the effect of the temperature-dependence of the dielectric function. We also underline the fact that the emission is not necessarily proportional to the surface nor to the volume of the particle. In a second step, we investigate the super-Planckian regime of homogeneous non-magnetic spheres as a function of the size parameters and of the permittivities. The results provide clear examples of the sizes at which the super-Planckian regime starts and clues on the optimal thermal power that can be extracted from an isolated compact object.

In order to quantify the heat emitted by a sphere, we consider a model[7,13] based on Mie theory[14] and fluctuational electrodynamics which gives a rigorous description of thermal emission by homogeneous spheres of arbitrary radii. The emitted thermal power is given by

$$Q = \int_0^\infty d\omega \Theta(\omega, T)\tau_s(\omega), \tag{1}$$

where $\Theta(\omega,T) = \frac{\hbar\omega}{e^{\frac{\hbar\omega}{k_B T}}-1}$ is the mean energy of the Planck oscillator at temperature T and

$$\tau_s = \frac{2}{\pi}\sum_{P=E,M}\sum_{l=1}^{\infty}(2l+1)\left[\mathrm{Re}(\mathcal{T}_l^P) - |\mathcal{T}_l^P|^2\right]. \tag{2}$$

$\mathcal{T}_l^P$ are the Mie coefficients for electric (E) and magnetic (M) multipoles of order l.[14] They are functions of the Mie parameters $X = \omega R/c$ and $Y = n(\omega, T)\omega R/c$, where R is the sphere radius, c is the speed of light in vacuum, and $n(\omega,T) = \sqrt{\epsilon(\omega,T)}$ is the relative refractive index of the non-magnetic sphere, known to be linked to the dielectric function (permittivity) ϵ. Note that ϵ depends on the frequency and that the temperature dependence is often omitted for the sake of simplicity. Equation (2) is proportional to the absorption cross-section obtained in Mie theory by integrating the Poynting vector over a surface surrounding the

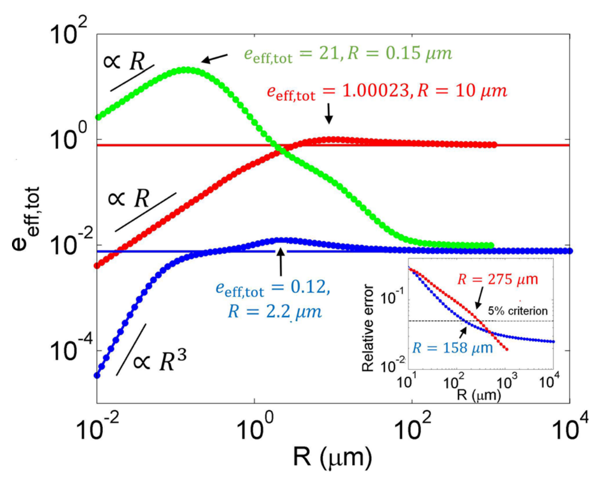

FIG. 1. Total effective emissivity $e_{\mathrm{eff,tot}} = Q/(4\pi R^2\sigma T^4)$ of spheres at $T = 300$ K as a function of their radius for different materials: gold (blue circles), SiO_2 (red circles), and constant dielectric function $\epsilon = -2 + 0.0238i$ (green circles). The horizontal lines are the results obtained with the macroscopic model for large spheres, and the dots are the results obtained with the wave model. The inset presents the relative errors between the macroscopic and the wave models. The arrows indicate the regions for which emission is higher than the Planck limit.

[a)]Electronic mail: khac-long.nguyen@insa-lyon.fr

sphere as described in Refs. 13 and 14. The term in $\mathrm{Re}(\mathcal{T}_l^P)$ originates from the extinction cross-section, while the one in $|\mathcal{T}_l^P|^2$ stems from the scattering cross-section. The signs of the Mie coefficients follow the definition of Ref. 14. The fact that the absorption cross-section appears here to describe emission is an expression of Lorentz reciprocity.

Figure 1 presents the total effective emissivity $e_{\mathrm{eff,tot}}$ at $T = 300\,\mathrm{K}$, defined as $Q/(4\pi R^2 \sigma T^4)$, of spheres obtained with the wave model (circles) with different material properties: gold, SiO_2, and constant permittivity $\epsilon = -2 + 0.0238i$ (grey material). $\sigma = \pi^2 k_B^4 / 60 c^2 \hbar^3$ is the Stefan-Boltzmann constant. The emissivities are termed as effective in the following because they are not necessarily surface quantities. Similar curves have been shown by Krüger *et al.*[13] Here, we have used the asymptotic formula of Bessel functions of the Mie coefficients to compute the total effective emissivity of very large spheres. The horizontal lines are the results obtained with the classical model for large spheres, which neglects interferences and diffraction. We remind that for large spheres, the surface can be considered as locally flat and the emission is the same as for a semi-infinite flat medium. As a consequence, no radius dependence is observed at large radii in Fig. 1. The macroscopic emission of a single sphere is the product of the surface area and Stefan's law $Q = 4\pi R^2 e \sigma T^4$, where e is the total hemispherical emissivity of the material. For grey materials, the emitted power is expected to be proportional to $R^2 T^4$. The inset presents the relative errors between the macroscopic and wave models for gold and SiO_2 spheres, which shows that the macroscopic model is no longer correct for microspheres ($R < 150\,\mu\mathrm{m}$ for a relative difference larger than 5%, the same criterion that was applied in Refs. 15 and 16). We warn that this value is much larger than $10\,\mu\mathrm{m}$, Wien's wavelength at room temperature, which is no more relevant because the spectrum differs from that of Planck's blackbody when departing from the macroscale. Interestingly, for small radii, we find that the total emitted power of gold spheres is proportional neither to R^3 nor to R^2; the emission is not proportional to the surface nor to the volume.

The size and temperature dependencies of the thermal emission of small spheres can be analyzed in more detail by approximating Eq. (1) to

$$Q = \int_0^\infty d\omega \Theta(\omega, T) \frac{\omega^3}{\pi^2 c^3} [\mathrm{Im}(\alpha_E) + \mathrm{Im}(\alpha_H)], \quad (3)$$

where the electric and magnetic polarisabilities α_p are given by[17]

$$\alpha_E = 4\pi R^3 \frac{\epsilon - 1}{\epsilon + 2}, \quad \alpha_H = \frac{2\pi}{15} R^3 \left(\frac{\omega R}{c}\right)^2 (\epsilon - 1). \quad (4)$$

For small metal spheres, the magnetic dipole dominates, and using the Drude model for the permittivity of Al, it can be shown that $\mathrm{Im}[\alpha_H(\omega)]$ is proportional to $R^5\omega$ at low frequencies and $R^5\omega^{-1}$ at high frequencies.[17] Their thermally radiated power Q is therefore proportional to $R^5 T^6$ at low temperatures and $R^5 T^4$ at high temperatures. This analysis confirms that the emission is not proportional to the volume. For small dielectric spheres, electric dipole dominates, and

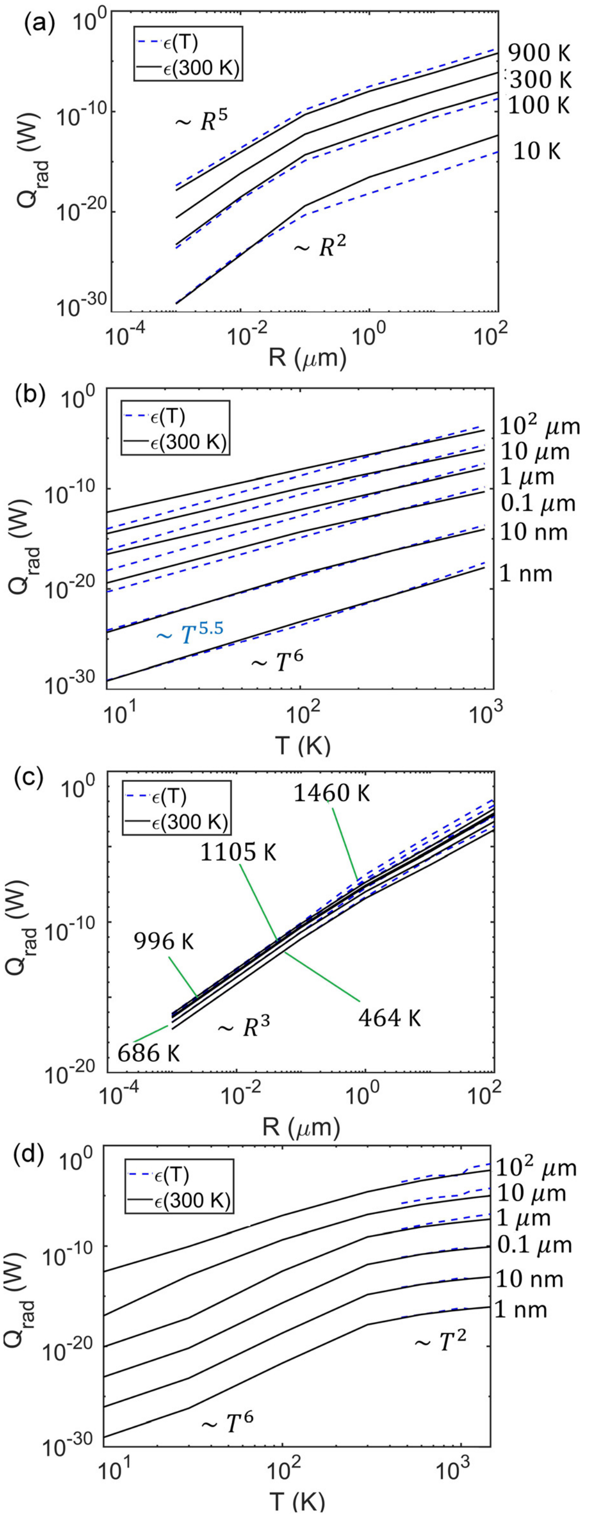

FIG. 2. Emitted thermal power of (a) and (b) Al and (c) and (d) SiC spheres for different radii and temperatures.

using the Lorentz model for the permittivity of SiC, it can be shown that $\mathrm{Im}[\alpha_E(\omega)]$ is approximated by $R^3\omega$ at low frequencies (below the resonance) and $R^3\omega^{-3}$ at high frequencies. The thermally emitted power Q is proportional to $R^3 T^6$ at low temperatures and to $R^3 T^2$ at high temperatures. Figure 2 shows the emitted power of Al and SiC spheres for radii ranging logarithmically between 1 nm and 10 μm with different temperatures. The results have been computed with Eqs. (1) and (2). The black curves represent the results for the

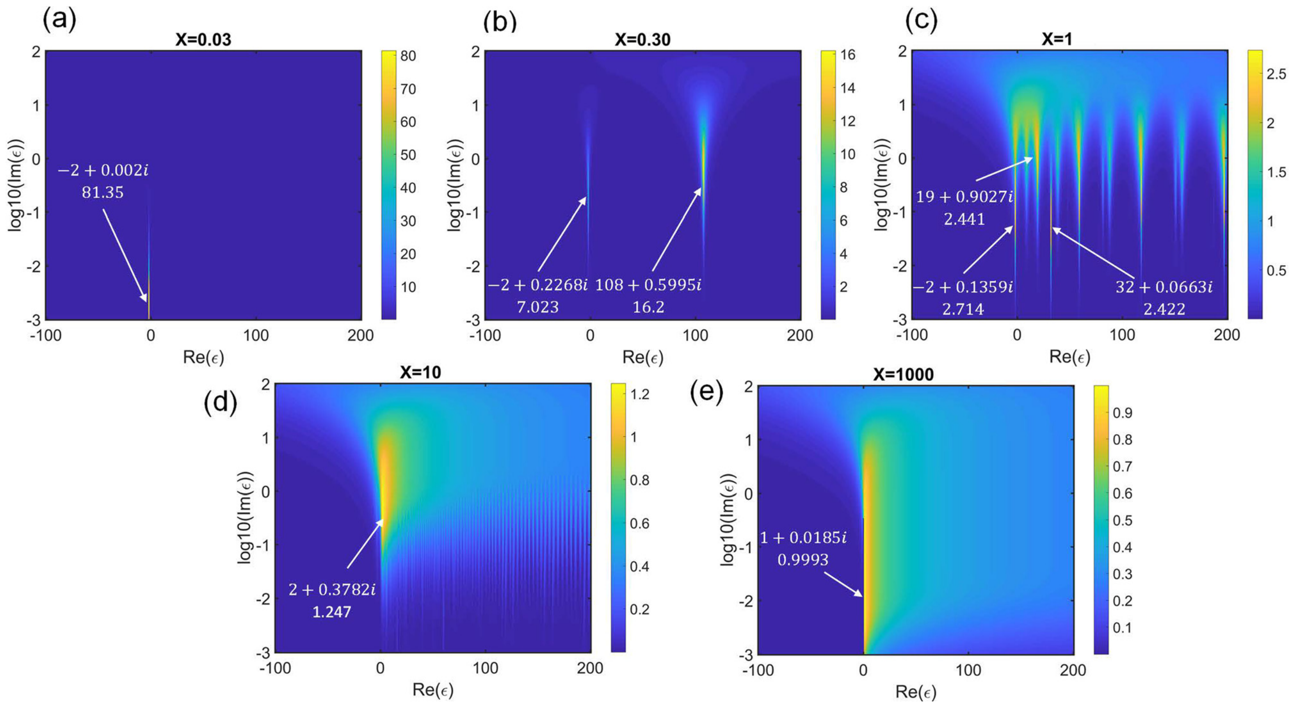

FIG. 3. Spectral effective emissivity of a sphere in the complex permittivity plane for different size parameters $X = \omega R/c$. Specific values of the permittivities and the associated maximal spectral effective emissivities are indicated (see supplementary material for a grayscale version of this figure).

permittivities that are independent of temperature, given by Drude and Lorentz models taken at room temperature. The predicted power laws mentioned before are indeed observed for the small radii in this case as well as for small gold and SiO_2 spheres in Fig. 1. The blue curves correspond to the results for dielectric functions depending on temperature. While all the data have not been measured in the whole range of computed temperatures, we include them by computing and extrapolating the data for aluminum as in Refs. 16 and 18 to high temperatures. For silicon carbide, the experimental data reported by De Sousa Meneses *et al.*, found, e.g., in Ref. 19, are considered for temperatures larger than 300 K. It is observed that the temperature dependence cannot be neglected in all cases. The effect can be a softening or a strengthening of the emission, depending on the temperature regime [see Fig. 2(b) for instance]. The emission of the spheres can be compared with those of other configurations. For instance, the total thermal emission by apertures much smaller than Wien's wavelength was found to be proportional to T^8 at low temperatures.[20] This could indicate that small objects emit drastically less than predictions from Stefan's law.

It is therefore interesting to observe in Fig. 1 that some spheres, i.e., finite objects, can radiate more energy than what an equivalent blackbody would ($e_{\mathrm{eff,tot}} > 1$).[7] For instance, the total effective emissivity of the SiO_2 sphere of radius 10 μm is slightly larger than 1. We acknowledge that the experimental data[21] of the dielectric function may not be accurate enough to be certain that the effective emissivity value is larger than 1. However, it is possible to increase largely such a value as shown by the constant permittivity material (green curve). In the following, we are interested in studying the variation of thermal emission of spheres as a function of their dielectric properties and radii. We note that the permittivities of such homogeneous spheres do not respect the Kramers-Kronig relations (KKR).[22] The values of ϵ that we find could serve as guides to determine possible KKR-compatible properties.

First of all, the influence of material properties on the spectral emissivity $e_{\mathrm{eff}}(\omega) = \pi\tau_s/X^2$ is investigated. Figure 3 presents the spectral emissivity of a sphere as a function of its complex permittivity ϵ for different size parameters $X = \omega R/c$. $\epsilon_{\max}$ values for which the effective emissivity shows local maxima in the complex permittivity plane are indicated with arrows. The impact of three kinds of Mie resonances can be observed.[14] Resonances associated with real parts of the permittivity close to -2 exist for a large range of size parameters. Their emissivities are dominant for small X [see Fig. 3(a) for $X = 0.03$] and much larger than one (blackbody emissivity for $X \to \infty$). These resonances are referred to as electric dipole

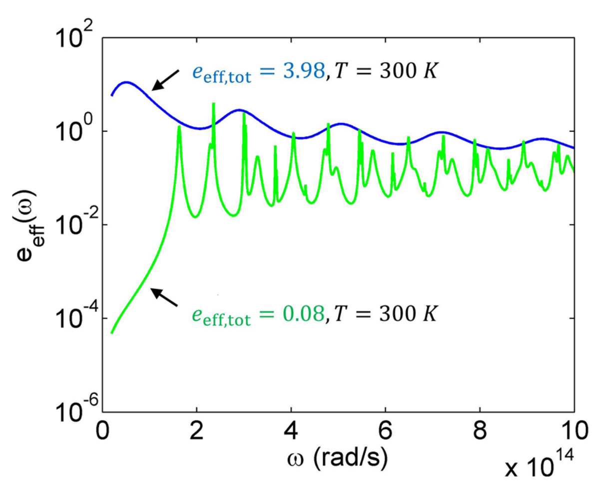

FIG. 4. Spectral effective emissivity of a sphere of 1 μm radius for a constant dielectric function $\epsilon(\omega) = -2 + 0.1359i$ (blue curve) and $\epsilon(\omega) = 32 + 0.0663i$ (green curve).

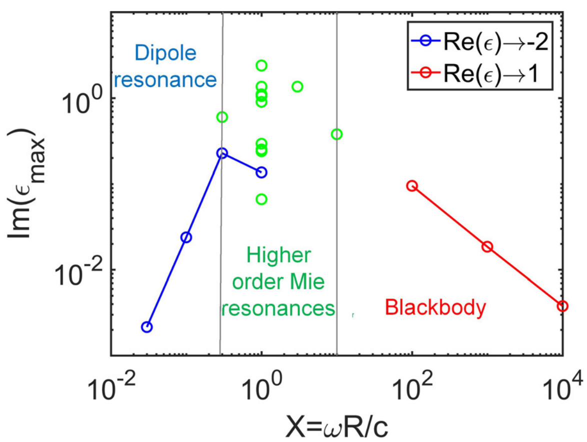

FIG. 5. Imaginary part of the dielectric constant that leads to resonances in Fig. 3, as a function of size parameter.

resonances. For large X, the emissivities at resonances associated with real parts of the permittivity approximately equal to one become dominant [see Fig. 3(e) for $X=10^3$] and close to the blackbody emissivity. The other resonances associated with real parts different from -2 and 1 appear in the transition regime ($X\sim 1$). Their spectral emissivities can be larger or smaller than those of the dipole resonances (see Fig. 3 for $X=0.3$ and $X=1$).

The effect of each kind of resonance on the emission is now investigated. In Fig. 4, we compare the spectral emissivity of a sphere of radius 1 μm for two different dielectric constants. The blue curve corresponds to a constant permittivity ($\epsilon_{\max}=-2+0.1359i$) associated with the dipole resonance, and the green curve corresponds to a constant permittivity ($\epsilon_{\max}=32+0.0663i$) associated with another resonance. Despite the fact that the radius is not always small compared to the wavelength, the dipole resonance provides a total emissivity larger than the other resonance in almost the whole frequency range and especially in the lower part of the spectrum. By contrast, $\mathrm{Re}(\epsilon)=32$ leads to sharp local peaks. In the end, the dipole resonance leads to the strongest total emission with $e_{\mathrm{eff,\,tot}}$ larger than 1.

Finally, Fig. 5 shows the imaginary parts leading to the maxima of emission as a function of size parameters (see Fig. 3 for the values of the maxima). They can be distinguished depending on the values of the real part of the permittivity associated with the different resonances [i.e., $\mathrm{Re}(\epsilon)=-2,\,1,\ldots$]. It is worth noting that a trend towards low values of $\mathrm{Im}(\epsilon_{\max})$ is observed for both small and large sizes. Figure 3(a) seems to indicate that the largest effective emissivities can be reached for the smallest objects. For large finite objects with $\mathrm{Re}(\epsilon)=1$, the maximal emission is achieved approximately for $\mathrm{Im}(\epsilon)\propto R^{-0.7}$. While it is known that the optimal emission is achieved for $\epsilon=1+i\alpha$, $\alpha\rightarrow 0$ if a semi-infinite medium is considered (perfect blackbody), it is not the case anymore for finite objects where the finite size leads to a finite value of $\mathrm{Im}(\epsilon)$ for maximizing the emission. This is due to the tradeoff between the transmission at the interface, which decreases if $\mathrm{Im}(\epsilon)$ increases, and the absorption in the volume, which increases if $\mathrm{Im}(\epsilon)$ increases.

In conclusion, we have investigated the different emitted power laws for metal and dielectric spheres of small and large radii. A simple method has been proposed for predicting results for permittivities independent of temperature. These behaviors are modified for dielectric functions depending on temperature. We have found that the usual emissivity concept, associated with the surface state of a given material, breaks down for particle radii smaller than 150 μm, and one option is to replace it by an effective emissivity which depends on the radius of the material. One original feature of low dimensions is that the total power emitted can be characterized by power laws as large as T^6. In addition, we have studied the thermal emission of non-magnetic homogeneous grey spheres as a function of their dielectric function and have shown super-Planckian emission. This regime can exist when the dielectric function is close to that of the dipole resonance, while the other Mie resonances do not lead to strong total emission even in the transition regime. In the future, it will be important to determine the impact of the shape, and not only the size, on the emission.

See supplementary material for a grayscale version of Fig. 3.

The authors acknowledge the support of Project No. EU FP7-NMP-2013-LARGE-7 QuantiHeat. They also acknowledge R. Vaillon for discussions.

[1]A. Babuty, K. Joulain, P.-O. Chapuis, J.-J. Greffet, and Y. de Wilde, Phys. Rev. Lett. **110**, 143103 (2013).
[2]K. Joulain, P. Ben-Abdallah, P.-O. Chapuis, C. Henkel, A. Babuty, and Y. de Wilde, J. Quant. Spectrosc. Radiat. Transfer **136**, 1–15 (2014).
[3]K. Kim, B. Song, V. Fernández-Hurtado, W. Lee, W. Jeong, L. Cui, D. Thompson, J. Feist, M. T. H. Reid, D. J. Garcia-Vidal, J. C. Cuevas, E. Meyhofer, and P. Reddy, Nature **528**, 387–391 (2015).
[4]A. Narayanaswamy, S. Shen, and G. Chen, Phys. Rev. B **78**, 115303 (2008).
[5]E. Rousseau, A. Siria, G. Jourdan, S. Volz, F. Comin, J. Chevrier, and J.-J. Greffet, Nat. Photonics **3**, 514 (2009).
[6]C. Sorensen, Aerosol Sci. Technol. **35**, 648–687 (2001).
[7]G. W. Kattawar and M. Eisner, Appl. Opt. **9**, 2685–2690 (1970).
[8]S.-A. Biehs and P. Ben-Abdallah, Phys. Rev. B **93**, 165405 (2016).
[9]J.-J. Greffet, P. Bouchon, G. Brucoli, E. Sakat, and F. Marquier, "Generalized Kirchhoff law," e-print arXiv:1601.00312.
[10]V. A. Golyk, M. Krüger, and M. Kardar, Phys. Rev. E **85**, 046603 (2012).
[11]I. S. Nefedov and L. A. Melnikov, Appl. Phys. Lett. **105**, 1610902 (2014).
[12]Z. Yu, N. P. Sergeant, T. Skauli, G. Zhang, H. Wang, and S. Fan, Nat. Commun. **4**, 1730 (2013).
[13]M. Krüger, G. Bimonte, T. Emig, and M. Kardar, Phys. Rev. B **86**, 115423 (2012).
[14]C. F. Bohren and D. R. Huffman, *Absorption and Scattering of Light by Small Particles* (Wiley-Interscience, New York, 1983).
[15]Y. Tsurimaki, P.-O. Chapuis, J. Okajima, A. Komiya, S. Maruyama, and R. Vaillon, J. Phys.: Conf. Ser. **676**, 012023 (2016).
[16]Y. Tsurimaki, P.-O. Chapuis, J. Okajima, A. Komiya, and S. Maruyama, J. Quant. Spectrosc. Radiat. Transfer **187**, 310–321 (2017).
[17]P.-O. Chapuis, M. Laroche, S. Volz, and J.-J. Greffet, Appl. Phys. Lett. **92**, 201906 (2008).
[18]E. Blandre, P.-O. Chapuis, and R. Vaillon, Opt. Express **24**, A374–A387 (2016).
[19]K. Joulain, Y. Ezzahri, J. Drévillon, B. Rousseau, and D. D. S. Meneses, Opt. Express **23**, A1388–A1397 (2015).
[20]K. Joulain, Y. Ezzahri, and R. Carminati, J. Quant. Spectrosc. Radiat. Transfer **173**, 1–6 (2016).
[21]E. D. Palik, *Handbook of Optical Constants of Solids* (Academic Press, Boston, 1985).
[22]J. S. Toll, Phys. Rev. **104**, 1760–1770 (1956).